

Deuteron-alpha scattering: separable vs nonseparable Faddeev approach

L. Hlophe^{(a),*}, Jin Lei^{(b),†}, Ch. Elster^(b), A. Nogga^(c), F.M. Nunes^(a), D. Jurčiukonis^(d), and A. Deltuva^(d)

(a) National Superconducting Cyclotron Laboratory and Department of Physics and Astronomy,

Michigan State University, East Lansing, MI 48824, USA

(b) Institute of Nuclear and Particle Physics,

and Department of Physics and Astronomy,

Ohio University, Athens, OH 45701, USA

(c) IAS-4, IKP-3, and JHCP,

Forschungszentrum Jülich, D-52428 Jülich, Germany

(d) Institute of Theoretical Physics and Astronomy,

Vilnius University, Vilnius, Lithuania

(Dated: July 4, 2019)

Background: Deuteron induced reactions are widely used to probe nuclear structure and astrophysical information. Those (d,p) reactions may be viewed as three-body reactions and described with Faddeev techniques.

Purpose: Faddeev-AGS equations in momentum space have a long tradition of utilizing separable interactions in order to arrive at sets of coupled integral equations in one variable. However, it needs to be demonstrated that observables calculated based on separable interactions agree exactly with those based on nonseparable forces.

Methods: Momentum space AGS equations are solved with separable and nonseparable forces as coupled integral equations.

Results: Deuteron-alpha scattering is calculated via momentum space AGS equations using the CD-Bonn neutron-proton force and a Woods-Saxon type neutron(proton)-⁴He force, for which the Pauli-forbidden S-wave bound state is projected out. Elastic as well as breakup observables are calculated and compared to results in which the interactions in the two-body sub-systems are represented by separable interactions derived in the Ernst-Shakin-Thaler (EST) framework.

Conclusions: We find that the calculations based on the separable representation of the interactions and the original interactions give results that are in excellent agreement. Specifically, integrated cross sections and angular distributions for elastic scattering agree within $\approx 1\%$, which is well below typical experimental errors. In addition, the five-fold differential cross sections corresponding to breakup of the deuteron agree extremely well.

PACS numbers: 24.10.-i, 25.45.De, 21.45.-v

arXiv:1907.01587v1 [nucl-th] 2 Jul 2019

* hlophe@nscl.msu.edu

† jinl@ohio.edu

I. INTRODUCTION

Nuclear reactions offer an excellent probe into the properties of nuclei, particularly for short-lived rare isotopes. Nuclear reactions are extremely proliferous: they provide access to structure properties that improve our knowledge of the underlying nucleon-nucleon (NN) force, they are used to populate excited states of interest, and through them we can extract astrophysical rates that cannot otherwise be directly measured. However, a common concern when using nuclear reactions to extract nuclear properties pertains to the simplifications in describing the dynamics and consequent model dependence of the extracted properties. For this reason, it is a priority that our field develops new methods for reactions that are not limited by unnecessary approximations. In short, the goal is for a theory that includes an exact treatment of the dynamics for the relevant degrees of freedom and incorporates the relevant reaction channels in a consistent framework and on an equal footing. In addition, this reaction theory should be applicable across the nuclear chart and for a wide range of energy regimes, so that it is not plagued by irreconcilable systematic differences [1]. This is the context of the present study. We focus first on deuteron induced reactions on the α -particle, but note that the framework is readily extendable to heavier projectiles.

While nuclear reactions are in a fundamental way many-body problems, in direct reactions, when only a few degrees of freedom play a role, the problem is often reduced to a few-body problem. As early as the pioneering work by Shanley [2], three-body approaches have been successfully used to simplify the nuclear reaction problem and allow for an exact treatment of the few-body dynamics. In Refs. [2, 3], three-body solutions of the Alt-Grassberger-Sandhas (AGS) equations [4] for the scattering of deuterons off an α -particle were obtained using rank-1 separable two-body forces. Both elastic scattering observables and the total breakup cross sections, $n+p+\alpha$, were computed and compared to experiment. Despite its simplicity, the model provided a fair description of the data.

In the last decade, the AGS equations were applied in the field of nuclear reactions by Deltuva and Fonseca [5, 6] without the need to employ separable interactions, given the advances in computational power. The greatest challenge however, when moving from applications in the few-nucleon sector to reactions with heavy ions concerns the Coulomb force. Deltuva and Fonseca relied on screening the Coulomb interaction and subsequent renormalization to ensure the compactness of the Faddeev equations. Over the last decade, there have been many applications of this approach on a variety of reactions, such as deuteron stripping and pickup reactions involving halo nuclei, with latest developments including also excitations of the nuclear core [7]. Albeit the success of the method, incorporating the Coulomb force still poses unwanted limitations: when it becomes too strong (i.e. for heavier nuclei and for lower scattering energies), the Coulomb screening radius needed for an accurate description of the reaction increases to a point that renders the screening method ineffective. In practice this means that the methods in [5–7] have been applied so far to targets with mass $A \leq 58$.

An alternative to introducing Coulomb screening in the AGS equations is to cast the AGS equations in the Coulomb basis. In Ref. [8], Mukhamedzhanov and collaborators derived the AGS equations in the Coulomb basis, indicating also the necessity for employing a separable expansion of the forces in the different subsystems. That work is focused on the formalism and includes no numerical applications. It thus remains to be proven that this alternative method indeed can provide precise solutions for deuteron induced reactions on heavy nuclei.

Our work represents an important stepping stone for using Faddeev techniques for nuclear reactions with heavy nuclei. Starting from the non-relativistic AGS equations [4], we make use of the formulation derived by Lovelace [9], and introduce pair-wise separable interactions as previously developed [10–12]. For the treatment of the singularities in the free three-body propagator above the breakup threshold, we implement a procedure proposed in [13, 14], which allows one to cast the so-called moving singularities (see e.g. [15]) into singularities depending only on one variable, amenable to regular subtraction techniques. In this work, we do not explicitly include target excitation in our formulation. However, the formalism readily extends to problems in which the two-body subsystems can be described as a coupled-channel problem involving the excitation of one of the bodies [16].

In few-nucleon physics, the use of separable interactions is widespread and has been proven to be accurate in describing neutron-deuteron processes below the pion threshold [17, 18]. It is important that these benchmarks be performed for nuclear reactions, where the interaction has larger complexity. Recently, we performed a benchmark for the bound state of ${}^6\text{Li}$ [12] and showed that one can obtain 4 digit accuracy in the binding energy if including rank-8 potentials. In the present work, we perform a similar benchmark but now for deuteron-alpha elastic scattering and breakup reactions. We compare the results obtained in the new framework using separable interactions with the solutions obtained when no separable expansion is introduced [5]. The current work includes only nuclear interactions to allow for a careful inspection of the treatment of the short range aspects of the problem. We will focus on the inclusion of Coulomb in a subsequent study.

The paper is organized in the following way. In Sec. II, a brief summary of the theory is provided, highlighting essential ingredients for our calculations. Section III introduces the two-body input to our calculations and presents deuteron-alpha scattering observables for elastic as well as breakup scattering together with essential convergence tests. We conclude in Sec. IV. A detailed description of our treatment of the three-body breakup singularities and

the calculation of the kinematical S-curve for three particles with different masses is given in the appendices.

II. FORMAL CONSIDERATIONS

For the description of the scattering of a deuteron off an alpha particle, we employ the Alt, Grassberger, and Sandhas (AGS) equations [19], which are Faddeev-type integral equations in momentum space for three-particle transition operators

$$U^{ij} = \bar{\delta}_{ij} G_0^{-1} + \sum_k \bar{\delta}_{ik} t_k G_0 U^{kj}. \quad (1)$$

Here $\bar{\delta}_{ij} = 1 - \delta_{ij}$ is the anti-Kronecker delta, $G_0(E) = (E + i0 - H_0)^{-1}$ is the free resolvent at the available three-particle center-of-mass energy E , and H_0 is the free three particle Hamiltonian. The three particles with masses m_i , m_j , and m_k and spins s_i , s_j , and s_k interact via pairwise forces $v^i \equiv v_{jk}$ ($i, j, k = 1, 2, 3$ and cyclic permutations thereof) so that the operator $t_i(E) = v^i + v^i G_0(E) t_i(E)$ describes the two-body t matrix in the subsystem i . The AGS transition amplitudes U^{ij} are represented in their natural Jacobi coordinates (p_i, q_i) , where p_i is the relative momentum of the i^{th} pair and q_i the momentum of the i^{th} particle (also called the ‘spectator’) relative to the pair. For solving the AGS equations, we choose a momentum space basis which depends on the magnitude of the momenta and angular momentum eigenstates. To proceed, we define the total spin $S_i = s_j + s_k$, relative orbital angular momentum l_i , and the total angular momentum by $J_i = l_i + S_i$ for the i^{th} pair. The orbital angular momenta and spin of the spectator are represented by λ_i and s_i so that the corresponding total angular momentum is $\mathcal{J}_i = \lambda_i + s_i$. The third component of the spectator spin is denoted by m_{s_i} . The total angular momentum of the three-particle system is represented by J and the third component by M_J . The states of conserved total angular momentum are thus given as

$$|p_i q_i \alpha_i\rangle = |p_i q_i (l_i(s_i s_j) S_i) J_i(\lambda_i s_i) \mathcal{J}_i) J M_J\rangle, \quad (2)$$

and are normalized as

$$\langle p'_i q'_i \alpha'_i | p_i q_i \alpha_i \rangle = \frac{\delta(p'_i - p_i) \delta(q'_i - q_i)}{p'_i p_i q'_i q_i} \delta_{\alpha'_i \alpha_i}. \quad (3)$$

The matrix elements of an AGS operator for the transition from an arrangement channel j to i is given by the expectation value $\langle \Phi_i | U^{ij} | \Phi_j \rangle$, where

$$|\Phi_i\rangle \equiv \sum_{l_i S_i} |\phi_{l_i S_i}^{J_i} (l_i S_i) J_i M_{J_i}\rangle |q_i s_i m_{s_i}\rangle, \quad (4)$$

is the asymptotic state in arrangement channel i with $|\phi_{l_i S_i}^{J_i}\rangle$ being the two-body bound state wavefunction.

Two approaches for solving Eqs. (1) are adopted. We shall refer to them as the ‘separable’ and the ‘non-separable’ approach. The former involves a separable expansion of the two-body t matrix while the latter does not. The non-separable method is taken over from Ref. [5] and calculates fully off-shell t matrices on the momentum grid, with subsequent interpolation using global spline functions whenever needed.

For the separable expansion method, the subsystem t matrices take the well known form (see e.g. [20])

$$t_i^{\alpha_i \alpha'_i}(E_{q_i}) = \sum_{mn} |h_m^{\alpha_i}\rangle \tau_{mn}^{\alpha_i \alpha'_i}(E_{q_i}) \langle h_n^{\alpha'_i} |, \quad (5)$$

where $|h_m^{\alpha_i}\rangle$ are the so-called form factors and $E_{q_i} \equiv E - q_i^2/2M_i$ represents the available two-body energy. Here M_k is the reduced mass of the pair and the spectator. The indices m, n represent the rank of the separable potential, and i stands for the arrangement channel. If the potential v^i supports a bound state, the corresponding wave-function has the form

$$|\phi_{\alpha_i}^i\rangle = \sum_m G_0(\epsilon_{\alpha_i}) |h_m^{\alpha_i}\rangle c_{m\alpha_i}, \quad (6)$$

where the two-body bound state energy is related to the on-shell spectator momentum q_{i0} by

$$\epsilon_{\alpha_i} = E_{q_{i0}} = E - \frac{q_{i0}^2}{2M_i}. \quad (7)$$

The constants $c_{m\alpha_i}$ are determined by substituting Eq. (6) into a bound state Lippmann-Schwinger equation. The partial wave matrix element for a transition from the bound state $|\phi_{\alpha_i}^i\rangle$ to $|\phi_{\alpha_j}^j\rangle$ becomes

$$\langle\phi_{\alpha_i}^i q_i \alpha_i | U^{ij} | \phi_{\alpha_j}^j q_j \alpha_j \rangle = \sum_{mn} c_{m\alpha_i}^* c_{n\alpha_j} \langle h_m^{\alpha_i} q_i \alpha_i | G_0(\epsilon_{\alpha_i}) U_{ij} G_0(\epsilon_{\alpha_j}) | h_n^{\alpha_j} q_j \alpha_j \rangle. \quad (8)$$

To proceed, one defines the effective two-body AGS transition amplitudes [19]

$$X_{m\alpha_i, n\alpha_j}^{ij}(q_i, q_j; E) \equiv \langle h_m^{\alpha_i} q_i \alpha_i | G_0(E) U^{ij} G_0(E) | h_n^{\alpha_j} q_j \alpha_j \rangle, \quad (9)$$

whose on-shell values coincide with those of Lovelace [21] and appear on the right-hand side of Eq. (8). From Eqs. (1), one obtains

$$\begin{aligned} \langle h_m^{\alpha_i} q_i \alpha_i | G_0(E) U^{ij} G_0(E) | h_n^{\alpha_j} q_j \alpha_j \rangle &= \bar{\delta}_{ij} \langle h_m^{\alpha_i} q_i \alpha_i | G_0(E) | h_n^{\alpha_j} q_j \alpha_j \rangle \\ &+ \sum_k \sum_{\alpha_k \alpha'_k} \bar{\delta}_{ik} \int dq_k q_k^2 \langle h_m^{\alpha_i} q_i \alpha_i | G_0(E) | q_k \alpha_k \rangle \langle q_k \alpha_k | t_k(E_{q_k}) | q_k \alpha'_k \rangle \\ &\times \langle q_k \alpha'_k | G_0(E) U^{kj} G_0(E) | h_n^{\alpha_j} q_j \alpha_j \rangle, \end{aligned} \quad (10)$$

and substituting the separable two-body t matrix yields

$$\begin{aligned} \langle h_m^{\alpha_i} q_i \alpha_i | G_0(E) U^{ij} G_0(E) | h_n^{\alpha_j} q_j \alpha_j \rangle &= \bar{\delta}_{ij} \langle h_m^{\alpha_i} q_i \alpha_i | G_0(E) | h_n^{\alpha_j} q_j \alpha_j \rangle \\ &+ \sum_k \sum_{\alpha_k \alpha'_k} \sum_{m'n'} \bar{\delta}_{ik} \int dq_k q_k^2 \langle h_m^{\alpha_i} q_i \alpha_i | G_0(E) | h_{m'}^{\alpha_k} q_k \alpha_k \rangle \tau_{m'n'}^{\alpha_k \alpha'_k}(E_{q_k}) \\ &\times \langle q_k \alpha'_k | h_{n'}^{\alpha'_k} | G_0(E) U^{kj} G_0(E) | h_n^{\alpha_j} q_j \alpha_j \rangle. \end{aligned} \quad (11)$$

Defining the effective two-body ‘transition potentials’

$$Z_{m\alpha_i, n\alpha_j}^{ij}(q_i, q_j, E) = \bar{\delta}_{ij} \langle h_m^{\alpha_i} q_i \alpha_i | G_0(E) | h_n^{\alpha_j} q_j \alpha_j \rangle, \quad (12)$$

and using Eq. (9), one can express Eqs. (11) in a condensed form

$$\begin{aligned} X_{m\alpha_i, n\alpha_j}^{ij}(q_i, q_j; E) &= Z_{m\alpha_i, n\alpha_j}^{ij}(q_i, q_j, E) + \sum_k \sum_{\alpha_k \alpha'_k} \sum_{m'n'} \int dq_k q_k^2 Z_{m\alpha_i, m'\alpha_k}^{ik}(q_i, q_k; E) \\ &\times \tau_{m'n'}^{\alpha_k \alpha'_k}(E_{q_k}) X_{n'\alpha'_k, n\alpha_j}^{kj}(q_k, q_j; E). \end{aligned} \quad (13)$$

These equations are solved using iterative Lanczos-type techniques [22]. The kernel contains two types of singularities, namely, the bound state pole and the three-body breakup singularity. On one hand, the former constitutes a simple pole and is removed using standard subtraction techniques. On the other hand, the three-body breakup pole has a complex structure and its treatment is consequently more involved. A detailed discussion is provided in Appendix A.

To evaluate the transition amplitude for a breakup process, we first define the on-shell momentum of the pair $p_{i0} = \sqrt{2\mu_i(E - q_i^2/2M_i)}$, where μ_i is the reduced mass of the pair. The on-shell breakup amplitude is then expressed in terms of the amplitudes for elastic scattering and rearrangement processes using Eq. (1) leading to

$$\langle q_i p_{i0} \alpha_i | U^{0j} | \Phi_j \rangle = \sum_{k=1}^3 \langle p_{0i} q_i \alpha_i | t_k G_0(E) U^{kj} | \Phi_j \rangle. \quad (14)$$

For separable two-body t matrices, one obtains

$$\langle q_i p_{i0} \alpha_i | U^{0j} | \Phi_j \rangle = \sum_{k=1}^3 \sum_{\alpha_k \alpha'_k} \sum_{mn'n} \int dp_k p_k^2 dq_k q_k^2 \langle q_i p_{i0} \alpha_i | q_k p_k \alpha_k \rangle h_m^{\alpha_k}(p_k) \tau_{mn'n}^{\alpha_k \alpha'_k}(E_{q_k}) X_{n'\alpha'_k, n\alpha_j}^{kj}(q_k, q_j; E) c_{n\alpha_j}. \quad (15)$$

The matrix elements $\langle q_i p_{i0} \alpha_i | q_k p_k \alpha_k \rangle$ describe a transformation between two Jacobi coordinates for $i \neq k$ and are evaluated as described in Ref. [23]. If $i = k$, these matrix elements reduce to the δ -functions of Eq. (3). It is thus seen that, once the effective two-body amplitudes X_{mn}^{ij} have been determined, the transition amplitudes for elastic scattering, as well as rearrangement and breakup processes can be readily computed.

III. RESULTS AND DISCUSSION

To demonstrate the accuracy of solving the Faddeev-AGS equations for deuteron-alpha scattering based on a separable expansion of the forces in the two-body subsystems, the convergence of the expansion must be tested and finally the converged calculation must be compared to a numerically converged calculation based on the non-separable version of the same forces. For this, we first define the three-body Hamiltonian with the forces in the different two-body subsystems, namely the neutron-proton (np) force and the effective interaction between a neutron or proton and the alpha-particle, i.e. the n/p - α forces. Then, elastic as well as breakup observables for d - α scattering are calculated, and their convergence with respect to the basis (rank) of the separable expansion is explored. Finally, the well-converged separable calculations are compared to the corresponding ones obtained with the non-separable forces in the subsystems.

A. Two-body input

For the np force, the high precision CD-Bonn [24] potential is adopted. As an effective interaction in the n/p - α system, we employ the Bang potential as given in Ref. [25] consisting of an attractive central Woods-Saxon and spin-orbit terms. The two-body model space is restricted to $l_i \leq 2$ for both the np and n/p - α systems. The Coulomb repulsion in the p - α system is omitted. The Bang potential supports a bound state in the n/p - α S-wave channel, which is removed with the projection technique described in [23].

For constructing separable representations for the two-body t matrices which enter the AGS equations, we employ the method suggested by Ernst, Shakin, and Thaler [20] (EST). The advantage of this scheme is that the t matrices calculated at specific energies with a given potential are taken as form factors of the separable expansion. While in [20] half-shell t matrices are used, an extension to using off-shell t matrices is straightforward [26]. The details on the explicit construction of the separable representations employed here are laid out in [27]. The application to the three-body calculation of the ${}^6\text{Li}$ bound state is presented in [23]. For the convenience of the reader, as well as to establish notation, essential ingredients are briefly repeated.

The EST approach applied in momentum space requires solving a two-body Lippmann-Schwinger (LS) equation at a specific scattering energy E_n with a given real (or complex) potential, leading to a t matrix $t(p, p_n; E_n)$. The on-shell t matrix corresponds to momentum $p_n = \sqrt{2\mu E_n}$. For all other values of p_n , the t matrix is fully off-shell. We use E_n (support energies) and p_n (support momenta) independently to construct the separable interactions. Thus any specific solution of the LS equation is characterized by the pair (E_n, p_n) , which we call an EST support point. Naturally, when E_n corresponds to a bound state energy in the two-body system, the t matrix is always fully off-shell. In Ref. [23], we calculated the three-body binding energy of ${}^6\text{Li}$ and found that by choosing p_n independently from the bound state energy, we could achieve better accuracy.

To ensure that the separable expansion converges, it is imperative to calculate observables using successively increasing ranks. For this reason, we define separable representations of the CD-Bonn and Bang potentials with ranks ranging from 3 to 7. Table I lists the EST support points used to construct the separable representations of the CD-Bonn potential, while Table II shows those for the Bang potential. The separable representations provide a good description of the two-body t matrix over a range of relative two-body energies E_2 which, in the context of solving the Faddeev-AGS equations, corresponds to $-\infty < E_2 \leq E$ (E being the three-body energy in the c.m. frame).

B. Deuteron-alpha scattering observables

The validity of the separable expansion depends on the beam energy for the reactions, thus we choose three deuteron beam energies, $E_d = 10, 20, \text{ and } 50$ MeV, for the benchmark calculations of the separable vs. non-separable solutions of the AGS equations. These energies cover the typical range for experiments of (d,p) reactions.

1. Integrated cross sections

Integrated cross sections are an important test of the calibration of our methods. We aim to achieve a precision of $\approx 1\%$ on this observables which is well below the typical experimental errors and the uncertainties associated with the two-body interactions. Tables III and IV show the integrated cross sections computed using the separable potentials given in Tables I and II at 10 and 20 MeV incident deuteron energy. We show results for separable potentials constructed only with support momenta obeying the constraint $p_n = \sqrt{2\mu|E_n|}$ (NN-EST3-1, NN-EST4-1, NN-EST5-1, NN-EST6-1, NN-EST7-1, NA-EST3-1, NA-EST4-1, NA-EST5-1, NA-EST6-1, and NA-EST7-1) as in [18]. We

also show results for separable potentials for which the support momenta p_n are independent from E_n (NN-EST6-2, NN-EST6-3, NN-EST7-2, NA-EST6-2, NA-EST6-3, and NA-EST7-2). These results are benchmarked against the integrated cross sections obtained using the non-separable approach, given in the bottom row. The first point to make is that a similar convergence rate is observed for both elastic and breakup cross sections. Moreover, the convergence pattern is similar for both the 10 and 20 MeV deuteron beam energies. The second point worth making is that, in this case, the inclusion of off-shell momenta does not represent an improvement of the restricted $p_n = \sqrt{2\mu|E_n|}$ basis, contrary to our observation for bound states. Thirdly, a rank-6 interaction already provides the desired level of precision. Finally, and most importantly, the results agree with the cross sections obtained from the non-separable calculation to $\approx 1\%$.

It is interesting to contrast our findings with those of Ref. [18] for nd scattering at 10 MeV incident neutron energy. In that work the authors demonstrated that an EST rank-3 potential could reproduce the integrated cross sections calculated using the non-separable method to about 2 %. From Tables III and IV, we see that the discrepancy between results calculated with the separable and non-separable approach is already better than $\sim 1.5\%$ for the rank-4 potentials, indicating that our findings are consistent with those of Ref. [18].

2. Elastic scattering: deuteron angular distributions

Next, we consider the differential cross sections for elastic deuteron-alpha scattering for three deuteron beam energies E_d . In Fig. 1, the differential cross sections for elastic $d + \alpha$ scattering as a function of the center-of-mass (c.m.) angle $\theta_{c.m.}$ are shown for three different incident deuteron energies, $E_d = 10, 20$ MeV, and 50 MeV. The solid lines indicate the angular distributions evaluated using the non-separable approach. The calculations obtained using rank-3, rank-4, and rank-5 separable potentials are indicated by the dash-dot-dotted, dash-dotted, and dashed lines. All four lines are nearly indistinguishable which demonstrates that the separable expansion is not only well-converged, but also yields deuteron angular distributions that are in excellent agreement with those obtained using the non-separable approach. The relative differences between the two results remain at $\approx 1\%$ throughout the angular range. This is well below the usual experimental uncertainties for this observable. It is worth noting that the separable expansion method is not limited to the low beam energies mentioned above. Increasing the beam energy by tens of MeV does not introduce any principal technical difficulties except that, obviously, the dependence on the rank of the separable expansion needs to be reevaluated.

3. Deuteron breakup: fivefold differential cross section

For an even more stringent test of the separable expansion method, we explore the convergence of the five-fold breakup differential cross section with respect to the rank of the separable expansion. Typically, one proceeds by specifying configurations defined by the outgoing proton and alpha particle angles (θ_p, ϕ_p) and $(\theta_\alpha, \phi_\alpha)$. The corresponding S-curves are then evaluated using energy and momentum conservation as described in Appendix B. Each configuration is given in the format $(\theta_\alpha, \phi_\alpha; \theta_p, \phi_p)$, with the angles given in degrees. We consider two configurations, one of which corresponds to the final state interaction (FSI). The FSI configurations are defined such that $E_{np} \approx 0$ for a single value of the arclength S . Here E_{np} is the relative energy between the outgoing neutron and proton.

Figure 2 displays the five-fold breakup differential cross section on the S-curve for $E_d = 10$ MeV for two different configurations of the $\alpha + n + p$ system. Panel (a) shows results for the configuration $(25.6^\circ, 0^\circ; 63.6^\circ, 180^\circ)$ while panel (b) depicts results for the FSI configuration $(31.4^\circ, 0^\circ; 5.1^\circ, 180^\circ)$. The cross sections computed with the non-separable method are indicated by the solid line. Results evaluated using the separable expansion method are depicted by the dash-dot-dotted, dash-dotted, and dashed lines for the rank-3, rank-4, and rank-5 potentials of Tables I and II. The FSI point is indicated by the filled square. The deviation of the dash-dot-dotted line from the other curves in both panels demonstrates that the rank-3 potential is inadequate for this observable. However, the separable expansion is still rapidly converging so that the rank-4 and rank-5 curves are virtually indistinguishable. We also observe that the converged results from the separable approach are in excellent agreement with those calculated using the non-separable method.

Next, we consider the five-fold breakup differential cross section at 20 MeV incident deuteron energy. Figure 3 is the same as Figure 2 but for $E_d = 20$ MeV. The configurations depicted in panels (a) and (b) are $(29.0^\circ, 0^\circ; 22.5^\circ, 180^\circ)$ and $(25.6^\circ, 0^\circ; 1.7^\circ, 180^\circ)$, where the latter corresponds to FSI. We note that the convergence pattern is similar to that of $E_d = 10$ MeV. Also, the rank-4 and rank-5 results are in very good agreement with those obtained via the non-separable approach.

In Section III B 2 we showed that the agreement between deuteron angular distributions calculated using the separable and non-separable methods remains excellent when the beam energy is increased to $E_d = 50$ MeV. For completeness, it is imperative that we also compare the five-fold breakup differential cross sections at this energy.

The comparison is shown in Fig. 4. Panel (a) depicts the configuration $(14.0^\circ, 0^\circ; 7.2^\circ, 180^\circ)$ while the off-plane configurations $(14.0^\circ, 0^\circ; 7.2^\circ, 120^\circ)$ and $(22.2^\circ, 0^\circ; 104.4^\circ, 100^\circ)$ are shown in panels (b) and (c). The FSI configuration $(22.2^\circ, 0^\circ; 104.4^\circ, 180^\circ)$ is illustrated in panel (d). The filled square indicates the FSI point. The solid line corresponds to results calculated using the non-separable approach while the dashed lines depicts those computed via the separable expansion method. We observe that the two methods are in excellent agreement and that the level of agreement is consistent with the one obtained for $E_d = 10$ and 20 MeV.

IV. SUMMARY AND OUTLOOK

Deuteron induced nuclear reactions are a widely used probe in nuclear physics. From a theoretical standpoint, these reactions are often mapped on a three-body problem $n + p + A$. The exact solution of the three-body problem can be obtained using the momentum-space Faddeev AGS framework. Given the long-range Coulomb force, the standard implementation of the AGS equations for deuteron induced nuclear reactions relies on the screening and renormalization method. However this limits the application to lighter targets and/or higher beam energies. To circumvent this limitation, one can instead use separable interactions and the Coulomb distorted basis as proposed in [8].

In this study, we implemented an AGS framework based on EST-like separable interactions, solved those separable AGS equations for scattering and constructed elastic and breakup observables. For the purpose of this benchmark, no Coulomb interactions were included. We applied our method to $d - \alpha$ scattering for $E_d = 10, 20, 50$ MeV, taking the same interactions as those used in a previous work where we benchmarked the use of separable interactions for three-body bound states [23]. We find that the new method converges well. Depending on the desired observable, rank-4 or rank-6 were sufficient for obtaining 1% precision.

For the benchmark, we also performed the AGS calculations using the non-separable interactions. The results obtained with the separable interactions agree very well with those using the standard non-separable AGS method. Specifically, the total cross sections and the elastic differential angular distributions calculated using these two methods agree to 1%. Breakup is typically harder to calculate precisely. For this reason, we selected a wide variety of configurations for proton and neutron angles in order to test the method in the most extreme limits. For all cases considered, we found that the five-fold differential breakup cross sections obtained using the separable framework for rank-4 was already in very good agreement with the results using the non-separable approach. Moreover, no special adjustment of the separable force was needed when going from the three-body bound state calculation to the scattering application.

Consistent with the conclusion from the study of ${}^6\text{Li}$ bound states [23], we here demonstrate that the separable formulation provides a reliable method to solve the three-body scattering problem. It is now possible to follow onto the final step of the process, namely the inclusion of the Coulomb potential by solving the Faddeev-AGS equations in the Coulomb basis.

Appendix A: Treatment of Three-Body Breakup Singularities

The kernel of Eqs. (13) contains bound state singularities as well as three-body breakup poles. The former are simple poles and can be removed from the kernel using standard subtraction procedures. The breakup singularity has a more complicated structure and its removal requires more work. To proceed, we first note that the matrix elements of the three-body propagator have the form

$$G_0(p_i, q_i; E) = \left[E - \frac{p_i^2}{2\mu_i} - \frac{q_i^2}{2M_i} + i0 \right]^{-1}, \quad (\text{A1})$$

and that the breakup pole is located at the on-shell pair momentum $p_{0i}^2(q_i) = 2\mu_i(E - q_i^2/2M_i)$, so that Eq. (A1) can be written as

$$G_0(p_i, q_i; E) = \frac{2\mu_i}{p_{0i}^2(q_i) - p_i^2 + i0}. \quad (\text{A2})$$

The breakup pole constitutes a ‘moving singularity’ due to its dependence on the spectator momentum and is the major cause of numerical difficulties for scattering energies above the three-body breakup threshold. The numerical

complications are manifest when attempting to compute the transition potentials via Eq. (12). Using the fact that

$$\langle p_i q_i \alpha_i | p_k q_k \alpha_k \rangle = \int_{-1}^1 dx G_{\alpha_i \alpha_k}(q_i, q_k, x) \frac{\delta(p_i - \pi_i(q_i, q_k, x))}{p_i^2} \frac{\delta(p_k - \pi_k(q_i, q_k, x))}{p_k^2}, \quad (\text{A3})$$

Eq. (12) can be expressed as

$$Z_{m\alpha_i, n\alpha_k}^{ik}(q_i, q_k, E) = \int_{-1}^1 dx h_m^{\alpha_i}(\pi_i) G_{\alpha_i \alpha_k}(q_i, q_k, x) G_0(\pi_i, q_i; E) h_n^{\alpha_k}(\pi_k), \quad (\text{A4})$$

where the shifted momenta $\pi_i = \sqrt{\beta^2 q_i^2 + q_k^2 + 2\beta q_i q_k x}$ and $\pi_k = \sqrt{q_i^2 + \eta^2 q_k^2 + 2\eta q_i q_k x}$. Here $\beta = \mu_i/m_k$ and $\eta = \mu_j/m_k$. Substituting Eq. (A2) into Eq. (A4) yields

$$Z_{m\alpha_i, n\alpha_k}^{ik}(q_i, q_k, E) = \int_{-1}^1 dx h_m^{\alpha_i}(\pi_i) G_{\alpha_i \alpha_k}(q_i, q_k, x) \frac{2\mu_i}{p_{0i}^2 - \pi_i^2(q_i, q_k, x) + i0} h_n^{\alpha_k}(\pi_k). \quad (\text{A5})$$

Defining

$$x_0 = \frac{p_{0i}^2 - \beta^2 q_i^2 - q_k^2}{2\beta q_i q_k}, \quad (\text{A6})$$

Eq. (A5) can be expressed in the form

$$Z_{m\alpha_i, n\alpha_k}^{ik}(q_i, q_k, E) = \int_{-1}^1 dx h_m^{\alpha_i}(\pi_i) G_{\alpha_i \alpha_k}(q_i, q_k, x) \frac{\mu_i}{\beta q_i q_k} \frac{1}{x_0 - x + i0} h_n^{\alpha_k}(\pi_k). \quad (\text{A7})$$

The presence of $1/(x_0 - x + i0)$ implies a logarithmic singularity which occurs only if q_i is below $q_{bi} = \sqrt{2M_i E}$ so that the on-shell momentum of the pair $p_{0i}(q_i) > 0$. The transition potentials are thus well-defined for $q_i > q_{bi}$ and can be computed in the usual manner according to Eq. (A4). For $q_i \leq q_{bi}$ the x -integration is singular and an appropriate regularization scheme can be applied for $|x_0| < 1$. Contrarily, the Cauchy principal value is undefined for $|x_0| = 1$ due to the presence of end point singularities. As a way forward, we substitute Eqs. (12) into the kernel of Eqs. (13) leading to

$$\begin{aligned} X_{m\alpha_i, n\alpha_k}^{ik}(q_i, q_k; z) &= Z_{m\alpha_i, n\alpha_k}^{ik}(q_i, q_k, E) + \sum_j \sum_{\alpha_j \alpha'_j} \sum_{m' n'} \bar{\delta}_{ij} \int dp_i p_i^2 dq_j q_j^2 dp_j p_j^2 h_m^{\alpha_i}(p_i) \frac{2\mu_j}{p_{0j}^2(q_j) - p_j^2 + i0} \\ &\times \langle q_i p_i \alpha_i | q_j p_j \alpha_j \rangle h_{m'}^{\alpha_j}(p_j) \tau_{m' n'}^{\alpha_j \alpha'_j}(E_{q_j}) X_{m' \alpha'_j, n\alpha_k}^{jk}(q_j, q_k; E). \end{aligned} \quad (\text{A8})$$

For the partial waves containing at least one two-body bound state, the coupling matrix takes the form

$$\tau_{m' n'}^{\alpha_j \alpha'_j}(E_{q_j}) \equiv \frac{2M_j}{q_{0j}^2 - q_j^2 + i0} \tilde{\tau}_{m' n'}^{\alpha_j \alpha'_j}(E_{q_j}), \quad (\text{A9})$$

so that

$$\begin{aligned} X_{m\alpha_i, n\alpha_k}^{ik}(q_i, q_k; z) &= Z_{m\alpha_i, n\alpha_k}^{ik}(q_i, q_k, E) + \sum_j \sum_{\alpha_j \alpha'_j} \sum_{m' n'} \bar{\delta}_{ij} \int dp_i p_i^2 dq_j q_j^2 dp_j p_j^2 h_m^{\alpha_i}(p_i) \frac{2\mu_j}{p_{0j}^2(q_j) - p_j^2 + i0} \\ &\times \langle q_i p_i \alpha_i | q_j p_j \alpha_j \rangle h_{m'}^{\alpha_j}(p_j) \frac{2M_j}{q_{0j}^2 - q_j^2 + i0} \tilde{\tau}_{m' n'}^{\alpha_j \alpha'_j}(E_{q_j}) X_{m' \alpha'_j, n\alpha_k}^{jk}(q_j, q_k; E). \end{aligned} \quad (\text{A10})$$

Furthermore, the coupling matrix for partial waves supporting more than one bound state can always be written as a sum of terms similar to the right-hand side of Eq. (A9) by utilizing the concept of partial fractions [13, 14]. The most general singularity structure of the kernel is of the form

$$\frac{2\mu_j}{p_{0j}^2(q_j) - p_j^2 + i0} \frac{2M_j}{q_{0j}^2 - q_j^2 + i0}. \quad (\text{A11})$$

The bound state pole is disentangled from the propagator singularity by using the partial fraction expansion

$$\frac{2\mu_j}{p_{0j}^2(q_j) - p_j^2 + i0} \frac{2M_j}{q_{0j}^2 - q_j^2 + i0} = \frac{1}{\frac{p_j^2}{2\mu_j} - \epsilon_{\alpha_j}} \frac{2\mu_j}{p_{0j}^2(q_j) - p_j^2 + i0} - \frac{1}{\frac{p_j^2}{2\mu_j} - \epsilon_{\alpha_j}} \frac{2M_j}{q_{0j}^2 - q_j^2 + i0}. \quad (\text{A12})$$

Since the factor $1/(\frac{p_i^2}{2\mu_j} - \epsilon_{\alpha_j})$ is non-singular, the desired separation of the singularities is achieved. Substituting Eq. (A12) into Eq. (A10) and using Eq. (A3) one obtains

$$\begin{aligned}
X_{m\alpha_i, n\alpha_k}^{ik}(q_i, q_k; E) &= Z_{m\alpha_i, n\alpha_k}^{ik}(q_i, q_k, E) + \sum_j \sum_{\alpha_j \alpha'_j} \sum_{m' n'} \bar{\delta}_{ij} \left\{ \right. \\
&\int dp_i p_i^2 dq_j q_j^2 dp_j p_j^2 \int_{-1}^1 dx h_m^{\alpha_i}(p_i) \frac{1}{\frac{p_i^2}{2\mu_j} - \epsilon_{\alpha_j}} \frac{2\mu_j}{p_{0j}^2(q_j) - p_j^2 + i0} h_{m'}^{\alpha_j}(p_j) G_{\alpha_i \alpha_j}(q_i, q_j, x) \\
&\times \frac{\delta(p_i - \pi_i(q_i, q_j, x))}{p_i^2} \frac{\delta(p_j - \pi_j(q_i, q_j, x))}{p_j^2} \tilde{\tau}_{m' n'}^{\alpha_j \alpha'_j}(E_{q_j}) X_{n' \alpha'_j, n\alpha_k}^{jk}(q_j, q_k; E) \\
&- \int dp_i p_i^2 dq_j q_j^2 dp_j p_j^2 \int_{-1}^1 dx h_m^{\alpha_i}(p_i) \frac{1}{\frac{p_i^2}{2\mu_j} - \epsilon_{\alpha_j}} \frac{2M_j}{q_{0j}^2 - q_j^2 + i0} h_{m'}^{\alpha_j}(p_j) G_{\alpha_i \alpha_j}(q_i, q_j, x) \\
&\times \left. \frac{\delta(p_i - \pi_i(q_i, q_j, x))}{p_i^2} \frac{\delta(p_j - \pi_j(q_i, q_j, x))}{p_j^2} \tilde{\tau}_{m' n'}^{\alpha_j \alpha'_j}(E_{q_j}) X_{n' \alpha'_j, n\alpha_k}^{jk}(q_j, q_k; E) \right\}. \tag{A13}
\end{aligned}$$

For the first term, we use the delta function to evaluate the p_j integral and convert the delta function in p_i to a delta function in x

$$\frac{\delta(p_i - \pi_i(q_i, q_j, x))}{p_i^2} = \frac{1}{\beta p_i q_i q_j} \delta(x - x_0). \tag{A14}$$

For the second term inside the curly brackets, we use the delta functions to evaluate the p_i, p_j integrals and perform the angular integration to obtain different transition potentials

$$\bar{Z}_{m\alpha_i, m' \alpha_j}^{ij}(q_i, q_j, E) \equiv \int_{-1}^1 dx h_m^{\alpha_i}(\pi_i) \frac{1}{\epsilon_{\alpha_j} + \frac{\pi_j^2}{2\mu_j}} h_{m'}^{\alpha_j}(\pi_j) G_{\alpha_i, \alpha_j}(q_i, q_j, x). \tag{A15}$$

Substituting Eqs. (A14) and (A15) into Eq. (A13), and using the fact that kinetic energy is the same in all three Jacobi coordinates leads to

$$\begin{aligned}
X_{m\alpha_i, n\alpha_k}^{ik}(q_i, q_k; E) &= Z_{m\alpha_i, n\alpha_k}^{ik}(q_i, q_k, E) + \sum_j \sum_{\alpha_j \alpha'_j} \sum_{m' n'} \bar{\delta}_{ij} \left\{ \right. \\
&\int dp_i p_i \frac{1}{\beta q_i} h_m^{\alpha_i}(p_i) \frac{2\mu_i}{p_{0i}^2(q_i) - p_i^2 + i0} \int_{q_j=|p_i - \beta q_i|}^{q_j=p_i + \beta q_i} dq_j q_j \frac{1}{\frac{p_j^2}{2\mu_j} - \epsilon_{\alpha_j}} h_{m'}^{\alpha_j}(\pi_j) G_{\alpha_i \alpha_j}(q_i, q_j, x_0) \\
&\times \tilde{\tau}_{m' n'}^{\alpha_j \alpha'_j}(E_{q_j}) X_{m' \alpha'_j, n\alpha_k}^{jk}(q_j, q_k; E) \\
&- \int dq_j q_j^2 \bar{Z}_{m\alpha_i, m' \alpha_j}^{ij}(q_i, q_j, E) \frac{2M_j}{q_{0j}^2 - q_j^2 + i0} \tilde{\tau}_{m' n'}^{\alpha_j \alpha'_j}(E_{q_j}) X_{n' \alpha'_j, n\alpha_k}^{jk}(q_j, q_k; E) \left. \right\}. \tag{A16}
\end{aligned}$$

For partial waves that do not support any two-body bound state, only the propagator singularity is present. To proceed, we define N_b as the number of partial waves that support at least one two-body bound state so that the

coupled equations for the transition amplitudes take the form

$$\begin{aligned}
X_{m\alpha_i, n\alpha_k}^{ik}(q_i, q_k; E) &= Z_{m\alpha_i, n\alpha_k}^{ik}(q_i, q_k, E) + \sum_j \left[\sum_{\alpha_j=1}^{N_{bj}} \sum_{\alpha'_j=1}^{N_{bj}} \sum_{m'n'} \bar{\delta}_{ij} \right\{ \\
&\int dp_i p_i \frac{1}{\beta q_i} h_m^{\alpha_i}(p_i) \frac{2\mu_i}{p_{0i}^2(q_i) - p_i^2 + i0} \int_{q_j=|p_i-\beta q_i|}^{q_j=p_i+\beta q_i} dq_j q_j \frac{1}{\frac{p_j^2}{2\mu_j} - \epsilon_{\alpha_j}} h_{m'}^{\alpha_j}(\pi_j) G_{\alpha_i \alpha_j}(q_i, q_j, x_0) \\
&\times \tilde{\tau}_{m'n'}^{\alpha_j \alpha'_j}(E_{q_j}) X_{m'\alpha'_j, n\alpha_k}^{jk}(q_j, q_k; E) \\
&- \int dq_j q_j^2 \bar{Z}_{m\alpha_i, n\alpha_j}^{ij}(q_i, q_j, E) \frac{2M_j}{q_{0j}^2 - q_j^2 + i0} \tilde{\tau}_{m'n'}^{\alpha_j \alpha'_j}(E_{q_j}) X_{n'\alpha'_j, n\alpha_k}^{jk}(q_j, q_k; E) \left. \right\} \\
&+ \sum_{\alpha_j > N_{bj}} \sum_{\alpha'_j > N_{bj}} \sum_{m'n'} \int dp_i p_i \frac{1}{\beta q_i} h_m^{\alpha_i}(p_i) \frac{2\mu_i}{p_{0i}^2(q_i) - p_i^2 + i0} \int_{q_j=|p_i-\beta q_i|}^{q_j=p_i+\beta q_i} dq_j q_j h_{m'}^{\alpha_j}(\pi_j) G_{\alpha_i \alpha_j}(q_i, q_j, x_0) \\
&\times \tau_{m'n'}^{\alpha_j \alpha'_j}(E_{q_j}) X_{n'\alpha'_j, n\alpha_k}^{jk}(q_j, q_k; E) \left. \right].
\end{aligned} \tag{A17}$$

At this point all the singularities of the kernel have been reduced to simple poles. Since none of them are end point singularities, they can be removed using standard subtraction techniques. The resulting integral equations with a regularized kernel can be readily solved using iterative Lanzcos-type techniques [22].

Appendix B: The S-curve for Particles with Different Masses

In a breakup configuration of three particles, the energy can be continuously distributed between the relative motion of the fragments. Conservation of energy and total momentum impose additional constraints on which breakup configurations are accessible. The kinematically allowed configurations can be described by a so-called S-curve. In the following, the analytical form of this S-curve for three particles with different masses is derived in the laboratory frame. This is an extension of the derivation presented in Ref. [28] where particles with identical masses were considered.

First, the phase space Φ is given in Jacobi coordinates $\{\vec{p}, \vec{q}\}$ as

$$\Phi = \int d\vec{p} d\vec{q} \delta(E - E_p - E_q), \tag{B1}$$

where the δ -function is required by energy conservation. The three-body energy in the c.m. frame is given by E and

$$\int d\vec{p} d\vec{q} = \int d\hat{p} d\hat{q} dE_p dE_q p q \mu_p \mu_q, \tag{B2}$$

with μ_p and μ_q being the reduced masses. After integrating over E_p , the phase space factor, Eq. (B1), takes the final form,

$$\Phi = \int d\hat{p} d\hat{q} dE_q p q \mu_p \mu_q. \tag{B3}$$

In the laboratory frame the momentum of the target is zero before the collision. We now write the phase-space factor Φ using the momenta \vec{k}_i , \vec{k}_j , and \vec{k}_k of the particles after the breakup. Imposing energy and momentum conservation Φ takes the form

$$\Phi = \int d\vec{k}_i d\vec{k}_j d\vec{k}_k \delta \left(E_{lab} - \frac{k_i^2}{2m_i} - \frac{k_j^2}{2m_j} - \frac{k_k^2}{2m_k} \right) \delta^3(\vec{P}_{lab} - \vec{k}_i - \vec{k}_j - \vec{k}_k), \tag{B4}$$

where \vec{P}_{lab} is the momentum of the incoming particle in the laboratory frame and E_{lab} is the total three body energy in the laboratory frame. For the deuteron induced reaction the relation

$$E_{lab} = E_{in}^{lab} + E_d = \frac{P_{lab}^2}{2m_d} + E_d \tag{B5}$$

holds, where E_{in}^{lab} is the energy of the projectile in the laboratory frame, m_d and E_d are the mass and binding energy of the dimer, respectively.

Making use of the momentum conserving δ -function, one can integrate over \vec{k}_j which leads to

$$\Phi = \int d\vec{k}_i d\vec{k}_k \delta(f(\vec{k}_i, \vec{k}_k)), \quad (\text{B6})$$

where

$$f(\vec{k}_i, \vec{k}_k) = E_{lab} - \frac{k_i^2}{2m_i} - \frac{k_k^2}{2m_k} - \frac{(\vec{P}_{lab} - \vec{k}_i - \vec{k}_k)^2}{2m_j}. \quad (\text{B7})$$

Using Eq. (B5) $f(\vec{k}_i, \vec{k}_k)$ can be written as

$$f(\vec{k}_i, \vec{k}_k) = E_d + E_{in}^{lab} - \frac{P_{lab}^2}{2m_j} - \frac{(m_i + m_j)k_i^2}{2m_i m_j} - \frac{(m_j + m_k)k_k^2}{2m_j m_k} + \frac{P_{lab}k_i\omega_i + P_{lab}k_k\omega_k - k_i k_k \omega}{m_j}, \quad (\text{B8})$$

with

$$\omega_i = \frac{\vec{P}_{lab} \cdot \vec{k}_i}{P_{lab} k_i} = \cos \theta_i, \quad (\text{B9})$$

$$\omega_k = \frac{\vec{P}_{lab} \cdot \vec{k}_k}{P_{lab} k_k} = \cos \theta_k, \quad (\text{B10})$$

$$\omega = \frac{\vec{k}_i \cdot \vec{k}_k}{k_i k_k} = \sin \theta_i \sin \theta_k \cos \Delta\varphi + \cos \theta_i \cos \theta_k, \quad (\text{B11})$$

where θ_i and θ_k are the polar angles associated the direction of \vec{k}_i and \vec{k}_k when assuming \vec{P}_{lab} as z -axis. The quantity $\Delta\varphi$ is the difference between the corresponding azimuthal angles.

By using the well-known property of the δ function, $\delta[g(x)] = \sum_i \frac{1}{|g'(x_i)|} \delta(x - x_i)$, it is easy to rewrite $f(\vec{k}_i, \vec{k}_k)$ in a more convenient form and integrate Eq. (B6) over k_i , which leads to

$$\Phi = \int d\hat{k}_i d\hat{k}_k dk_k \frac{m_i m_j k_i^2 k_k^2}{|k_i(m_i + m_j) - m_i P_{lab} \omega_i + m_i k_k \omega|}. \quad (\text{B12})$$

For each value of k_k and the direction \hat{k}_i and \hat{k}_k , k_i is obtained from the solution of

$$E_d + E_{in}^{lab} - \frac{P_{lab}^2}{2m_j} - \frac{(m_i + m_j)k_i^2}{2m_i m_j} - \frac{(m_j + m_k)k_k^2}{2m_j m_k} + \frac{P_{lab}k_i\omega_i + P_{lab}k_k\omega_k - k_i k_k \omega}{m_j} = 0. \quad (\text{B13})$$

In the same way, it is possible to integrate Eq (B6) over k_k instead of k_i , and obtain

$$\Phi = \int d\hat{k}_i d\hat{k}_k dk_i \frac{m_j m_k k_i^2 k_k^2}{|k_k(m_k + m_j) - m_k P_{lab} \omega_k + m_k k_i \omega|}. \quad (\text{B14})$$

From Eqs. (B12) and (B14), one gets

$$\frac{m_i dk_k}{|k_i(m_i + m_j) - m_i P_{lab} \omega_i + m_i k_k \omega|} = \frac{m_k dk_i}{|k_k(m_k + m_j) - m_k P_{lab} \omega_k + m_k k_i \omega|}. \quad (\text{B15})$$

Since the energy E_i of particle i is given by $E_i = \frac{k_i^2}{2m_i}$, we have $dE_i = \frac{k_i}{m_i} dk_i$, and the expression above can be rewritten as

$$\frac{k_i dE_k}{|k_i(m_i + m_j) - m_i P_{lab} \omega_i + m_i k_k \omega|} = \frac{k_k dE_i}{|k_k(m_k + m_j) - m_k P_{lab} \omega_k + m_k k_i \omega|}. \quad (\text{B16})$$

We now define \mathcal{S} as

$$d\mathcal{S} = \sqrt{(dE_i)^2 + (dE_k)^2}, \quad (\text{B17})$$

which leads to the expression for phase space in laboratory frame

$$\Phi = \int d\hat{k}_i d\hat{k}_k d\mathcal{S} K_s, \quad (\text{B18})$$

with

$$K_s = \frac{m_i m_j m_k k_i^2 k_k^2}{\sqrt{k_i^2 |k_k(mk + mj) - m_k P_{lab} \omega_k + m_k k_i \omega|^2 + k_k^2 |k_i(m_i + m_j) - m_i P_{lab} \omega_i + m_i k_k \omega|^2}}. \quad (\text{B19})$$

In this work the d - α breakup reaction is characterized by the incident energy of the projectile in the laboratory frame E_{in}^{lab} , the polar angles θ_i and θ_k of the particles observed after the breakup, and the difference between the corresponding two azimuthal angles $\Delta\varphi$. To obtain the cross section as a function of \mathcal{S} , one needs to determine the values of k_i and k_k which are related through Eq. (B13). After some algebra the above equation can be cast into the form of an ellipse, whose characteristic equation is given by

$$\frac{x^2}{a^2} + \frac{y^2}{b^2} = 1 \quad (\text{B20})$$

with

$$\begin{bmatrix} x \\ y \end{bmatrix} = \begin{bmatrix} \cos \tilde{\theta} & -\sin \tilde{\theta} \\ \sin \tilde{\theta} & \cos \tilde{\theta} \end{bmatrix} \begin{bmatrix} k_i - k_i^c \\ k_k - k_k^c \end{bmatrix}. \quad (\text{B21})$$

Here $\tilde{\theta}$ is the angle of rotation, k_i^c and k_k^c are the center points for the k_i and k_k axes. These values are given by

$$\tilde{\theta} = \frac{1}{2} \arctan\left(\frac{2m_i m_k \omega}{m_j(m_i - m_k)}\right), \quad (\text{B22})$$

$$k_i^c = \frac{P_{lab} m_i (\omega_k \omega m_k - \omega_i (m_j + m_k))}{m_i m_k \omega^2 - (m_i + m_j)(m_j + m_k)}, \quad (\text{B23})$$

$$k_k^c = \frac{P_{lab} m_k (\omega_i \omega m_i - \omega_k (m_j + m_i))}{m_i m_k \omega^2 - (m_i + m_j)(m_j + m_k)}, \quad (\text{B24})$$

and the axes of the ellipse a and b are given by

$$a = \sqrt{\frac{\frac{m_j + m_i}{2m_i} k_i^c{}^2 + \frac{m_j + m_k}{2m_k} k_k^c{}^2 + k_i^c k_k^c \omega + m_j E_d - \frac{P_{lab}^2 m_i}{2m_d}}{\frac{m_j(m_i + m_k) + 2m_i m_k}{4m_i m_k} - \frac{\omega}{2 \sin(2\tilde{\theta})}}}, \quad (\text{B25})$$

$$b = \sqrt{\frac{\frac{m_j + m_i}{2m_i} k_i^c{}^2 + \frac{m_j + m_k}{2m_k} k_k^c{}^2 + k_i^c k_k^c \omega + m_j E_d - \frac{P_{lab}^2 m_i}{2m_d}}{\frac{m_j(m_i + m_k) + 2m_i m_k}{4m_i m_k} + \frac{\omega}{2 \sin(2\tilde{\theta})}}}. \quad (\text{B26})$$

By using the parametric form for an ellipse, k_i and k_k can be written as

$$k_i = a \cos t \cos \tilde{\theta} + b \sin t \sin \tilde{\theta} + k_i^c, \quad (\text{B27})$$

$$k_k = -a \cos t \sin \tilde{\theta} + b \sin t \cos \tilde{\theta} + k_k^c, \quad (\text{B28})$$

where t is the angular parameter. Making use of the two equations above, we can write the arc length \mathcal{S} as

$$d\mathcal{S} = \sqrt{\frac{k_i^2}{m_i^2} (-a \sin t \cos \tilde{\theta} + b \cos t \sin \tilde{\theta})^2 + \frac{k_k^2}{m_k^2} (a \sin t \sin \tilde{\theta} + b \cos t \cos \tilde{\theta})^2} dt. \quad (\text{B29})$$

Therefore, the arc length \mathcal{S} can be obtained as a function of t from the expression

$$\mathcal{S}(\tilde{t}) = \int_{t_0}^{\tilde{t}} \sqrt{\frac{k_i^2}{m_i^2} (-a \sin t \cos \tilde{\theta} + b \cos t \sin \tilde{\theta})^2 + \frac{k_k^2}{m_k^2} (a \sin t \sin \tilde{\theta} + b \cos t \cos \tilde{\theta})^2} dt. \quad (\text{B30})$$

ACKNOWLEDGMENTS

This work was performed in part under the auspices of the National Science Foundation under contract NSF-PHY-1520972 with Ohio University and NSF-PHY-1520929 with Michigan State University, of the U. S. Department of Energy under contract No. DE-FG02-93ER40756 with Ohio University, and of DFG and NSFC through funds provided to the Sino-German CRC 110 “Symmetries and the Emergence of Structure in QCD” (NSFC Grant No. 11621131001, DFG Grant No. TRR110), and by the ExtreMe Matter Institute EMMI at the GSI Helmholtzzentrum für Schwerionenphysik, Darmstadt, Germany. This research used resources of the National Energy Research Scientific Computing Center (NERSC), a U.S. Department of Energy Office of Science User Facility operated under Contract No. DE-AC02-05CH11231. This work was supported in part by Michigan State University through computational resources provided by the Institute for Cyber-Enabled Research. The work of A.Deltuva was supported by the Alexander von Humboldt-Foundation under Grant No. LTU-1185721-HFST-E

-
- [1] L. Atar *et al.*, Phys. Rev. Lett. **120**, 052501 (2018).
 - [2] P. E. Shanley, Phys. Rev. **187**, 1328 (1969).
 - [3] K. Miyagawa, Y. Koike, T. Ueda, T. Sawada, and S. Takagi, Prog. Theor. Phys. **74**, 1264 (1985).
 - [4] E. Alt, P. Grassberger, and W. Sandhas, Nuclear Physics B **2**, 167 (1967).
 - [5] A. Deltuva, Phys. Rev. C **74**, 064001 (2006).
 - [6] A. Deltuva and A. C. Fonseca, Phys. Rev. C **79**, 014606 (2009).
 - [7] A. Deltuva, D. Jurčiukonis, and E. Norvaišas, Phys. Lett. B **769**, 202 (2017).
 - [8] A. M. Mukhamedzhanov, V. Eremenko, and A. I. Sattarov, Phys. Rev. C **86**, 034001 (2012).
 - [9] C. Lovelace, Phys. Rev. **135**, B1225 (1964).
 - [10] L. Hlophe, C. Elster, R. C. Johnson, N. J. Upadhyay, F. M. Nunes, G. Arbanas, V. Eremenko, J. E. Escher, and I. J. Thompson (TORUS Collaboration), Phys. Rev. C **88**, 064608 (2013).
 - [11] L. Hlophe, V. Eremenko, C. Elster, F. M. Nunes, G. Arbanas, J. E. Escher, and I. J. Thompson (TORUS Collaboration), Phys. Rev. C **90**, 061602 (2014).
 - [12] L. Hlophe, J. Lei, C. Elster, A. Nogga, and F. M. Nunes, Phys. Rev. C **96**, 064003 (2017).
 - [13] H. Witala and W. Glöckle, Eur. Phys. J. **A37**, 87 (2008), arXiv:0806.2757 [nucl-th].
 - [14] C. Elster, W. Glöckle, and H. Witala, Few Body Syst. **45**, 1 (2009), arXiv:0807.1421 [nucl-th].
 - [15] W. Glöckle, *The Quantum Mechanical Few-Body Problem*, Texts and Monographs in Physics (Springer Verlag, 1983).
 - [16] L. Hlophe and C. Elster, Phys. Rev. C **95**, 054617 (2017).
 - [17] S. Nemoto, K. Chmielewski, N. W. Schellingerhout, J. Haidenbauer, S. Oryu, and P. U. Sauer, Few-Body Systems **24**, 213 (1998).
 - [18] T. Cornelius, W. Glöckle, J. Haidenbauer, Y. Koike, W. Plessas, and H. Witala, Phys. Rev. **C41**, 2538 (1990).
 - [19] E. O. Alt, P. Grassberger, and W. Sandhas, Nucl. Phys. **B2**, 167 (1967).
 - [20] D. J. Ernst, C. M. Shakin, and R. M. Thaler, Phys.Rev. **C8**, 46 (1973).
 - [21] C. Lovelace, Phys.Rev. **135**, B1225 (1964).
 - [22] Y. Saad, *Iterative Methods for Sparse Linear Systems* (Society for Industrial and Applied Mathematics, SIAM, 2003).
 - [23] L. Hlophe, J. Lei, C. Elster, A. Nogga, and F. M. Nunes, Phys. Rev. **C96**, 064003 (2017).
 - [24] R. Machleidt, Phys. Rev. **C63**, 024001 (2001).
 - [25] I. J. Thompson, B. V. Danilin, V. D. Efros, J. S. Vaagen, J. M. Bang, and M. V. Zhukov, Phys. Rev. C **61**, 024318 (2000).
 - [26] D. J. Ernst, C. M. Shakin, and R. M. Thaler, Phys.Rev. **C9**, 1780 (1974).
 - [27] L. Hlophe *et al.* (The TORUS Collaboration), Phys.Rev. **C88**, 064608 (2013).
 - [28] E. Garrido, A. Kievsky, and M. Viviani, Phys. Rev. **C90**, 014607 (2014), arXiv:1407.0172 [nucl-th].
 - [29] J. Bang and C. Gignoux, Nucl. Phys. **A313**, 119 (1979).

label	rank	support energy E_n [MeV]	support momenta p_n [fm^{-1}]
NN-EST3-1	3	-20, -2, 20	0.7 0.2, 0.5
NN-EST4-1	4	-60, -20, 10, 50	1.2, 0.7, 3.0, 0.8
NN-EST5-1	5	-80, -40, -5, 10, 50	1.4, 1.0, 0.3, 0.3, 0.8
NN-EST6-1	6	-100, -60, -2, 10, 35, 50	1.6, 1.2, 0.2, 0.3, 0.7, 0.8
NN-EST6-2	6	-20, -20, -20, -3, -3, -3	0.4, 0.7, 1.1, 0.4, 1.1, 2.5
NN-EST6-3	6	-20, -20, -20, 30, 30, 30	0.4, 0.7, 1.1, 0.4, 1.1, 2.5
NN-EST7-1	7	-150, -50, -25, -2, 10, 35, 75	2.4, 1.4, 1.0, 0.3, 0.6, 1.0, 1.2
NN-EST7-2	7	-20, -20, -20, -2, -3, -3, -3	0.2, 0.4, 1.1, 3.0, 0.4, 1.0, 3.0

TABLE I. Separable expansion of the CD-Bonn [24] potential. The labels and ranks are listed in the first and second column. The corresponding support energies and momenta are given in the third and fourth columns.

label	rank	support energy E_n [MeV]	support momenta p_n [fm^{-1}]
NA-EST3-1	3	-50, 10, 15	1.4, 0.6, 0.7
NA-EST4-1	4	-50, -5, 10, 35	1.4, 0.4, 0.6, 1.0
NA-EST5-1	5	-80, -40, -1, 10, 50	1.8, 1.2, 0.2, 0.6, 1.2
NA-EST6-1	6	-140, -100, -60, -20, -20, 40	2.3, 2.0, 1.5, 0.9, 0.8, 1.1
NA-EST6-2	6	-25, -25, -25, -5, -5, -5	0.4, 1.1, 2.0, 0.4, 1.1, 2.0
NA-EST6-3	6	-25, -25, -25, 35, 35, 35	1.0, 1.2, 3., 1.0, 2.0, 3.0
NA-EST7-1	7	-150, -50, -25, -2, 10, 35, 75	2.4, 1.4, 1.0, 0.3, 0.6, 1.0, 1.2
NA-EST7-2	7	-20, -20, -20, -2, -3, -3, -3	0.2, 0.4, 1.1, 3., 0.4, 1.0, 3.0

TABLE II. Separable expansion of the Bang potential [29]. The labels and ranks are listed in the first and second column. The corresponding support energies and momenta are given in the third and fourth columns.

potential		cross section [mb]		
np	n/p- α	elastic	breakup	total
NN-EST3-1	NA-EST3-1	789.1	492.3	1281.4
NN-EST4-1	NA-EST4-1	782.8	503.7	1286.5
NN-EST5-1	NA-EST5-1	780.9	502.4	1283.3
NN-EST6-1	NA-EST6-1	780.9	505.7	1286.5
NN-EST7-1	NA-EST7-1	781.0	503.9	1284.9
NN-EST6-2	NA-EST6-2	780.9	504.2	1285.1
NN-EST6-3	NA-EST6-3	781.0	504.2	1285.2
NN-EST7-2	NA-EST7-2	780.6	503.9	1284.5
CD-Bonn	Bang	781.8	505.8	1287.6

TABLE III. The integrated cross sections for $d+\alpha$ scattering obtained with the separable potentials of Tables I and II at 10 MeV incident deuteron energy. The potentials for the np and n/p- α reactions are given in the first and second columns, respectively. The cross section for elastic scattering and deuteron breakup are listed in the third and fourth columns while the total cross section is presented in the last column. and fourth columns. The exact results obtained using the original CD-Bonn and Bang interaction are displayed in the last row.

potential		cross section [mb]		
np	n/p- α	elastic	breakup	total
NN-EST3-1	NA-EST3-1	814.6	540.8	1355.4
NN-EST4-1	NA-EST4-1	812.1	540.9	1353.0
NN-EST5-1	NA-EST5-1	811.0	540.3	1351.5
NN-EST6-1	NA-EST6-1	810.6	541.7	1352.3
NN-EST7-1	NA-EST7-1	808.2	543.2	1351.5
NN-EST6-2	NA-EST6-2	810.5	541.7	1352.2
NN-EST6-3	NA-EST6-3	810.2	541.6	1351.8
NN-EST7-2	NA-EST7-2	810.4	541.6	1352.0
CD-Bonn	Bang	809.2	542.5	1351.6

TABLE IV. Same as Table III but for 20 MeV incident deuteron energy.

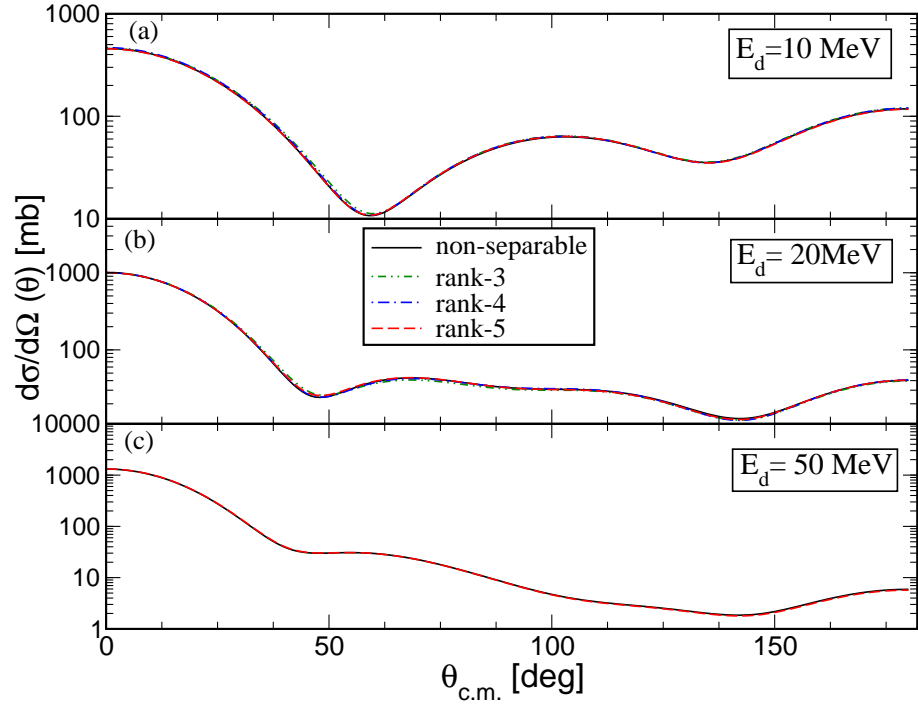


FIG. 1. The differential cross section for elastic deuteron-alpha scattering as a function of the center-of-mass angle $\theta_{c.m.}$. Panels (a) and (b) display results for the incident deuteron energies $E_d = 10$ and 20 MeV as indicated in the figure. The solid curve shows cross sections computed using the non-separable approach. The results calculated with the rank-3, rank-4, and rank-5 potentials are illustrated by the dot-dot-dashed, dot-dashed, and dashed curves. Panel (c) depicts the differential cross section at $E_d = 50$ MeV. The solid and dashed curves indicate the converged results evaluated via the separable and non-separable approach.

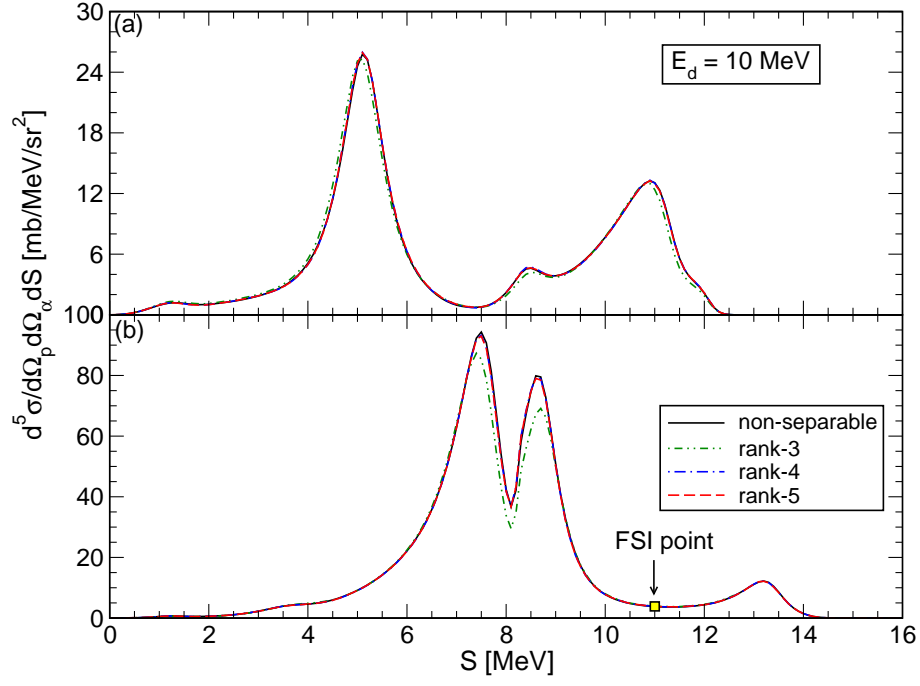


FIG. 2. The five-fold differential cross section for deuteron-alpha scattering as a function of the arc-length S at 10 MeV incident deuteron energy. Panel (a) shows results for the configuration $(25.6^\circ, 0^\circ; 63.6^\circ, 180^\circ)$ while panel (b) depicts results for the FSI configuration $(31.4^\circ, 0^\circ; 5.1^\circ, 180^\circ)$. The solid line corresponds to results calculated using the non-separable approach while the ones computed via the separable expansion method are illustrated by the dash-dot-dotted, dash-dotted, and dashed lines for the rank-3, rank-4, and rank-5 separable potentials, respectively. The QFS and FSI points are indicated by the symbols.

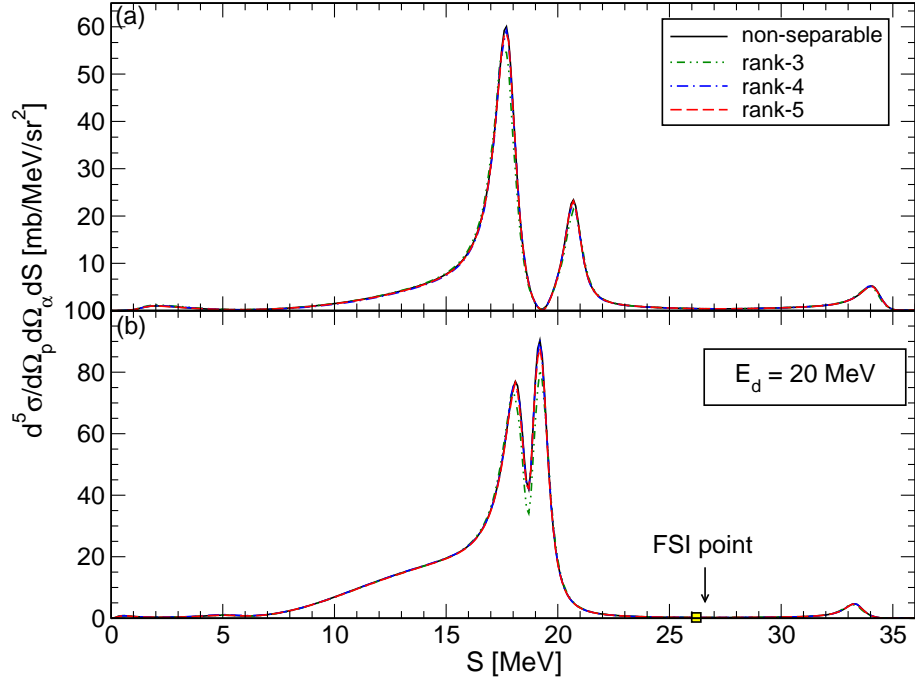


FIG. 3. Same as Fig. 2 but for 20 MeV incident deuteron energy. Panel (a) shows results for the configuration $(29.0^\circ, 0^\circ; 22.5^\circ, 180^\circ)$ while panel (b) depicts results for the FSI configuration and $(25.6^\circ, 0^\circ; 1.7^\circ, 180^\circ)$.

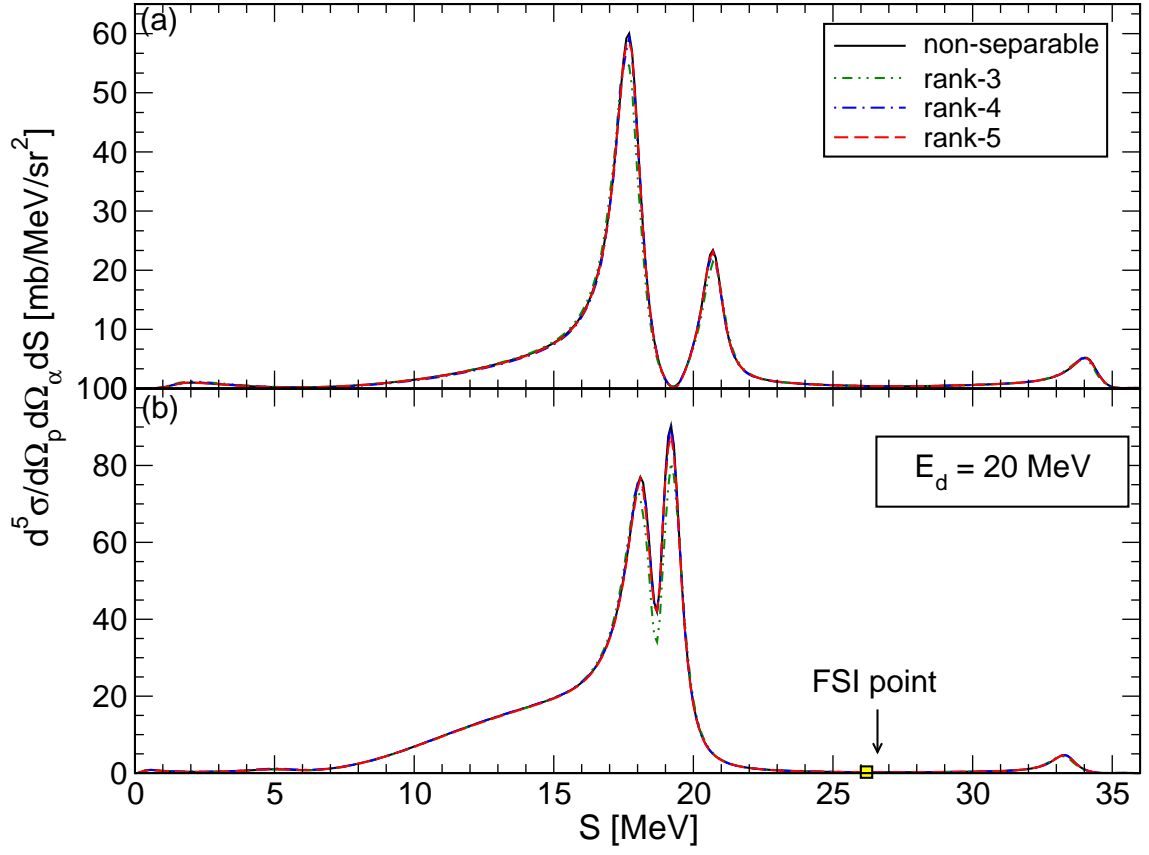


FIG. 4. The five-fold differential cross section for deuteron-alpha scattering as a function of the arc-length S at 50 MeV incident deuteron energy. Panel (a) depicts the configuration $(14.0^\circ, 0^\circ; 7.2^\circ, 180^\circ)$ while the off-plane configurations $(14.0^\circ, 0^\circ; 7.2^\circ, 120^\circ)$ and $(22.2^\circ, 0^\circ; 104.4^\circ, 100^\circ)$ are shown in panels (b) and (c). The FSI configuration $(22.2^\circ, 0^\circ; 104.4^\circ, 180^\circ)$ is illustrated in panel (d) and the FSI point is indicated by the filled square. The solid line corresponds to results calculated using the non-separable approach while the dashed lines depicts those computed via the separable expansion method.